Reduction of PV Module Temperature using Thermally Conductive Backsheets

Jaewon Oh, Balamurali Rammohan, Ashwini Pavgi, Sai Tatapudi, Govindasamy Tamizhmani, George Kelly, and Michael Bolen

Abstract-Photovoltaic (PV) modules typically operate at approximately 30 °C above ambient temperature on clear sunny days, irrespective of their location. Since the average annual daytime temperature is typically higher than 20 °C in most locations where PV modules are installed, operating temperatures can exceed 50 °C on clear sunny days. This translates to a 12 % reduction in nameplate power for crystalline silicon modules. In addition, thermally induced degradation mechanisms have a higher probability of occurrence when operating temperatures increase, thereby reducing the module lifetime. The operating temperatures are impacted by the selection of packaging materials, e.g., backsheets and encapsulants. This paper demonstrates a significant reduction in the operating temperature of single-cell modules with innovative thermally conductive backsheet (TCB) materials vis-à-vis baseline Tedlar/polyester/Tedlar (TPT) backsheet. **Field** results demonstrate that the nominal operating cell temperature (NOCT) of the TCB coupons is approximately 1 °C lower than those of conventional TPT coupons. The daily average module operating temperature of TCB coupons was as much as 3 °C cooler compared to the TPT coupons in summer months. Reducing the module temperature by 3 °C results in a 1.5 % relative efficiency increase. Finally, an empirical thermal model to predict the cell temperature for each backsheet type and a physical thermal model using ANSYS were developed and presented in this paper.

Index Terms—Backsheet, thermal conductivity, photovoltaic modules, NOCT, thermal model.

I. INTRODUCTION

It is well known that photovoltaic (PV) module performance depends on the operating temperature—the most important parameter influencing PV cell efficiency. The lower cell operating temperature, the higher is its efficiency [1]. The three most important extrinsic parameters influencing the packaged PV module temperature are the ambient temperature (temperature-increasing influence with increasing value), irradiance (temperature-increasing influence with increasing value), and wind speed (temperature-decreasing influence with increasing value). In a packaged PV module, the temperature-increasing influence with increasing value due to ambient

temperature and irradiance can be decreased, and the temperature-decreasing influence with increasing value caused by wind speed can be increased through careful selection of the non-cell module material properties. In this study, thermally conductive or radiative materials such as encapsulants and backsheets are explored.

To date, common module-cooling approaches use active cooling (e.g., pumping water through pipes on the back of modules or corrugated heat sinks) [2]-[4], which often adds more system costs than benefits. The module operating temperature also can be passively lowered by module encapsulation materials that have a high thermal conductivity [5], [6], selective-spectral cooling [7], [8], or increased radiative cooling [7], [9], [10]. This paper proposes a passive approach to relatively reduce the nominal operating cell temperature (NOCT) of flat-plate crystalline silicon (c-Si) modules by incorporating a thermally conductive backsheet (TCB). The most commonly used PV backsheet material has been polyvinyl fluoride (PVF; DuPont trade name "Tedlar")based backsheet, which typically has three layers: Tedlarpolyethylene terephthalate (PET)-Tedlar (=TPT). Compared to conventional TPT backsheets, TCB can passively reduce the module temperature, which could equate to 2 % more power and, theoretically, 30 % longer module lifetime [11]. Increasing a module's operating temperature reduces its power output due to an increase in the semiconductor's intrinsic carrier density, leading to a reduction in the open-circuit voltage and, subsequently, reducing the maximum power point voltage. Module manufacturers measure this effect with the "temperature coefficient" that estimates the relative efficiency loss for every degree Celsius a module operates above standard test conditions (STC), i.e., 25 °C. For c-Si PV modules, the temperature coefficient is typically -0.45 %/°C regarding the overall power [12]. For example, a rooftop module operating at 92 °C in a desert climate would output approximately 30 % less power compared to operating at STC. Therefore, reducing the operating temperature lowers the levelized cost of electricity (LCOE) via increased energy production (i.e., more kWh over the life of the asset) and increased service lifetime (years in the field) [11].

Manuscript submitted March 6, 2018. This material is based upon work supported by the U.S. Department of Energy's the Photovoltaic Research and Development (PVRD) program under Award Number DE-EE0007548.

J. Oh, B. Rammohan, A. Pavgi, S. Tatapudi, G. Tamizhmani are with Arizona State University Photovoltaic Reliability Laboratory, Mesa, AZ 85212 USA (e-mail: Jaewon.Oh@asu.edu; bnatara4@asu.edu; Ashwini.Pavgi@asu.edu; Sai.Tatapudi@asu.edu; manit@asu.edu).

M. Bolen is with Electric Power Research Institute, Charlotte, NC 28262 USA. (e-mail: mbolen@epri.com).

G. Kelly is with Sunset Technology, Mount Airy, MD 21771 USA. (e-mail: solarexpert13@gmail.com).

In this paper, we address lowering the cell temperature using backsheet materials with high thermal conductivities. It has been reported that conventional Tedlar-based backsheets have a lower thermal conductivity (0.2–0.3 W/m·K) than module encapsulation materials as well as solar cells [13], [14]. We present the effects of TCB on the PV module temperature by analyzing the NOCT and time series of the module operating temperature as well as the thermal conductivity of individual backsheets.

II. EXPERIMENTS

For this study, single-cell PV coupons/modules were fabricated using typical commercially available PV module encapsulation materials. The single-cell coupon structure replicates the typical commercial PV module stack: glass superstrate/ethylene-vinyl acetate copolymer encapsulant/cell/EVA encapsulant/backsheet or glass substrate. Low-iron solar glass (203 mm × 280 mm × 3.2 mm) and fastcure EVA (thickness: 0.46 mm) were used as superstrate and encapsulant, respectively. Industry-standard commercial 156 mm × 156 mm p-type mono-crystalline silicon aluminum backsurface field solar cells were used. Three different types of backsheet materials were selected for this study as shown in Fig. 1. A conventional TPT backsheet (thickness: 0.34 mm) was used as a reference/baseline material, and TCBs from two different manufacturers (TCB-A and TCB-B) were selected to compare the thermal performance between all three backsheets. polyvinylidene TCB-A layers of has fluoride (PVDF)/PET/EVA, and TCB-B consists of polyamide (PA)/aluminum/PET/PA. The color of the TPT and TCB

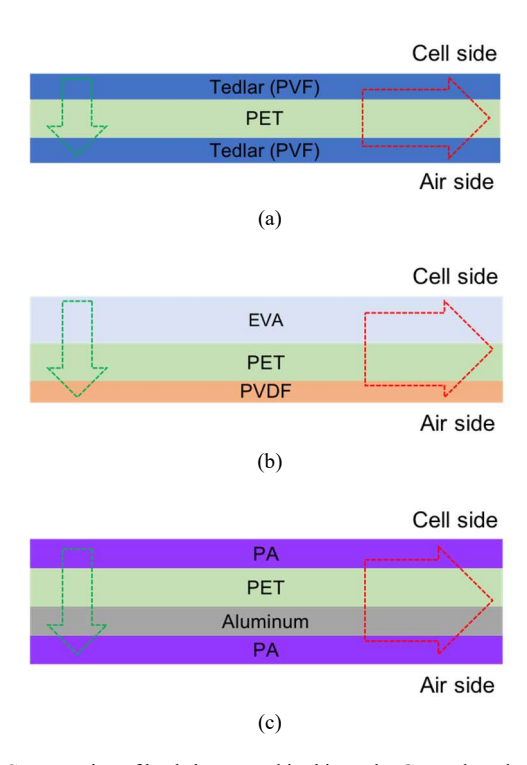


Fig. 1. Cross section of backsheets used in this study. Green dotted arrow and red dotted arrow represent axial (through-plane) thermal conductivity and radial (in-plane) thermal conductivity, respectively. Note that heat is originated from cell side. (a) TPT, (b) TCB-A, (c) TCB-B.

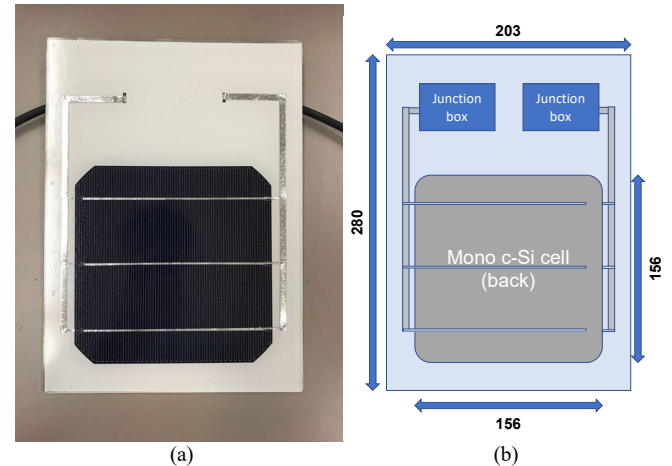


Fig. 2. Single-cell coupon (a) photograph (front), (b) dimension in millimeter (back).



Fig. 3. NOCT test rack and single-cell coupons installed in Mesa, Arizona, USA. (Coupon identification from left to right: TCB-A, TCB-A, TCB-B, TCB-B, TPT, TPT, glass/glass, and glass/glass)

materials is white on both sides. The thicknesses of TCB-A and TCB-B are 0.32 mm and 0.39 mm, respectively. In addition, a glass substrate—again made of low-iron glass—instead of a backsheet material was used in the single-cell coupon fabrication to investigate the effects of the substrate type (backsheet vs. glass) on the PV module temperature. The cell contacts were made by soldering 60Sn/40Pb tabbing ribbon with a semiautomatic tabbing machine onto the busbars of the solar cells. The single-cell coupon lamination was carried out at 150 °C for both glass/TPT and glass/glass coupons, as recommended by the EVA manufacturer. Single-pole junction boxes were attached to the back of the single-cell coupon using silicone (PV-804) sealant. A close-up photograph and the dimensions of the single-cell coupon are shown in Fig. 2(a) and (b), respectively. To measure the cell temperature, calibrated Ttype thermocouples with less than 0.3 °C uncertainty at 45 °C with extremely thin wires (36 AWG) were attached to the back of the solar cell prior to lamination. Additional thermocouples (30 AWG) were attached to the back of the single-cell coupons (on the backsheet) to measure the module temperature (backsheet temperature). Further, eight single-cell coupons encapsulated with various backsheet materials and glass

(2×TPT, 2×TCB-A, 2×TCB-B, and 2×Glass) were installed on an open rack following NOCT test conditions [15]: southfacing and 45° tilt, as shown in Fig. 3. Along with the cell and backsheet temperatures, weather data including plane of array (POA) irradiance measured by a pyranometer, ambient temperature, wind speed, and wind direction were also collected every 30 s by a Campbell Scientific CR1000 datalogger. The NOCT values for all samples were determined based on the IEC 61215 standard [15]. The thermal conductivity of the backsheet samples were measured at room temperature (24 °C) with a Hot Disk TPS 2500 S thermalconductivity meter, which can differentiate between axial (through-plane) and radial (in-plane) thermal conductivity (see Fig. 1). Since the thickness of the TCB is too small for the thermal-conductivity meter to effectively measure the thermal conductivity, a stack of multiple backsheets with handtightened screw pressure was applied to measure the thermal conductivity in accordance with the procedure recommended by the manufacturer. The specific heat capacity needed to determine the thermal conductivity in the TPS 2500 S was measured by using a differential scanning calorimeter. Emissivity measurement was carried out for all the backsheets used in this study. Further, the backsheet reflectance was determined by using an ultraviolet-visible-near infrared spectrophotometer. The backsheet reflectance inside (cell side) was measured through the glass on the non-cell area of the laminated single-cell coupon. An empirical thermal model was developed using a linear-regression approach to determine the quantitative influence of ambient conditions (POA irradiance, ambient temperature, and wind speed) on the cell temperature. Simple 2D steady-state thermal model at NOCT testing condition was developed using ANSYS for single-cell module. Material properties and boundary conditions were obtained using the literature [16], [17] and measured data shown in Tables I and II.

III. RESULTS AND DISCUSSION

A. Thermal conductivity of backsheets

Anisotropic thermal-conductivity measurements were carried out since all backsheet materials are made of 2-4 different polymeric layers. The thermal conductivity of the TCB and TPT backsheets are presented in Table I. An average of three measurements for each sample is presented in Table I with a relative standard deviation of less than 0.4 %. Evidently, TCB materials tend to have higher thermal conductivities than TPT materials. The measured axial thermal conductivity of TPT (0.153 W/m·K) is lower than the one reported for Tedlar-based backsheets with an aluminum interlayer [13], [18]. The highest thermal conductivity, including axial and radial, among the backsheet materials was observed for TCB-B. The axial thermal conductivity of TCB-B is approximately two times higher than that of TPT. It should be noted that the radial thermal conductivity of TCB-B is 13.53 W/m·K, which is extremely high compared to the values of the other two backsheet materials, glass (0.98 W/m·K), and encapsulant (0.23 W/m·K)

TABLE I THERMAL CONDUCTIVITIES OF THREE DIFFERENT TYPES OF BACKSHEET MATERIAL MEASURED AT 24 $^{\circ}\mathrm{C}$

Backsheet Type	Axial Thermal Conductivity (W/m·K)	Radial Thermal Conductivity (W/m·K)
TPT	0.153	0.486
TCB-A	0.259	0.371
TCB-B	0.382	13.53

[5]. This is attributed to the special structure of TCB-B, which possesses a very thin aluminum layer between the inner and outer polymer layers as shown in Fig. 1 (c). It was observed that TCB-A has a 69% higher axial thermal conductivity than TPT. However, its radial thermal conductivity is 24% lower than that of TPT. The effects of the thermal conductivity on the cell and module temperatures are presented in the following sections. It can be observed that the magnitude and direction of heat dissipation heavily depends on the material and stack structure of the backsheet. The magnitude and direction of thermal conductivity cannot be solely responsible for influencing the cell temperature within a module, which we elaborate on in later sections. Both thermal conductivity and material type affect thermal-radiative loss due to the material emissivity. Hence, they are important points to consider in the development of future PV products used to passively lower the operating temperature.

B. NOCT

The actual thermal performance of the backsheet materials in the packaged PV module was evaluated by determining the NOCT of each single-cell coupon. The latter was calculated by taking the average NOCT value measured during three clear sunny days. There exist two single-cell coupons from each substrate group. Thus, the NOCT of each of the two coupons was averaged to present the final NOCT values shown in Fig. 4. The average NOCT of the TCB coupons is lower than that of the TPT coupons. The NOCT of TCB-A and TCB-B are 1.2 °C and 0.7 °C lower than that of the conventional TPT coupons, respectively. These results are not consistent with a previous study (based on thermal simulations) [8] in which it was concluded that an increasing thermal conductivity of the backsheet leads to an improvement of no greater than 0.2 °C.

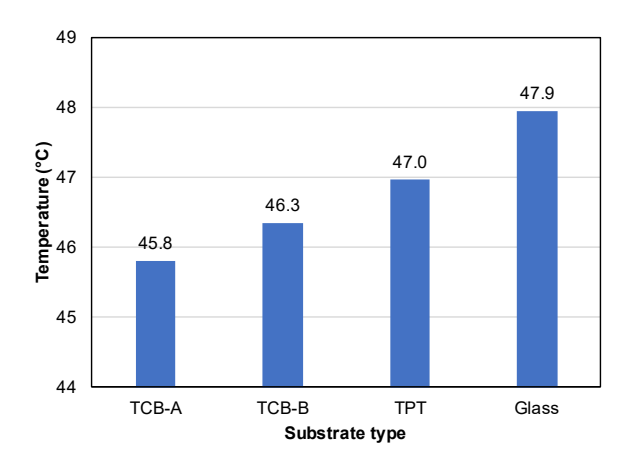


Fig. 4. NOCT values of single-cell coupons encapsulated with various substrates.

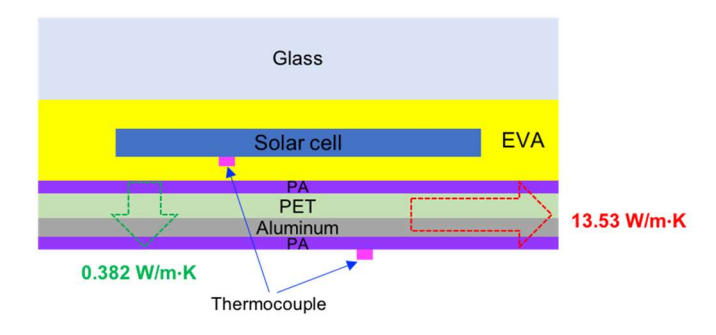


Fig. 5. Schematic drawing of TCB-B including thin aluminum layer used single-cell PV module. Green dotted arrow and red dotted arrow represent axial and radial thermal conductivity, respectively. Two thermocouples (one on back of solar cell and another on the backsheet) are used to calculate $\Delta T_{\text{C-BS}}$, a temperature difference between cell and backsheet.

TABLE II EMISSIVITY OF THREE DIFFERENT TYPES OF BACKSHEET MATERIAL MEASURED AT 27 $^{\circ}$ C

Backsheet Type	Hemispherical Total Emissivity			
TPT	0.830			
TCB-A	0.918			
TCB-B	0.806			

The lowest NOCT was observed for TCB-A and not for TCB-B samples, even though the latter exhibits a higher measured thermal conductivity than TCB-A.

However, this small test pool of samples is not sufficient to consider the enhanced thermal conductivity being caused by only the innovative material, since other material properties also affect the NOCT. For example, the results could potentially be attributed to the thin inner aluminum layer in the TCB-B material as shown in Fig. 5. Although the aluminum layer provides very high thermal conductivity compared to polymeric material [19], it also appears to block the radiative heat loss from the hot cell (i.e., aluminum has a low emissivity), resulting in a higher cell temperature compared to that of the backsheet without aluminum layer [20]. Table II shows that TCB-B has a lower emissivity due to the aluminum layer than TPT backsheet while TCB-A has higher emissivity than TPT. We also observed that adding aluminum layer between PVDF layer and PET layer in TCB-A lowers the emissivity (not shown here). TCB-B backsheet including aluminum layer facilitates heat conduction (due to high thermal conductivity) leading to smaller temperature difference between cell and backsheet (ΔT_{C-BS}) compared to ΔT_{C-BS} of TPT and TCB-A [21]. However, it reduces radiative heat loss due to the aluminum layer [20], which is why TCB-B cannot lower the cell temperature as much as TCB-A although it has higher thermal conductivity compared to TPT and TCB-A. Therefore, it is concluded that increasing the axial thermal conductivity without blocking the radiative heat would lead to lower operating temperatures in the modules.

Fig. 6 shows the reflectance of the three backsheet materials obtained on the non-cell area of the coupon through the glass superstrate. Among these backsheets, TCB-A shows the lowest reflectance within mid-infrared range (above 2000 nm). This

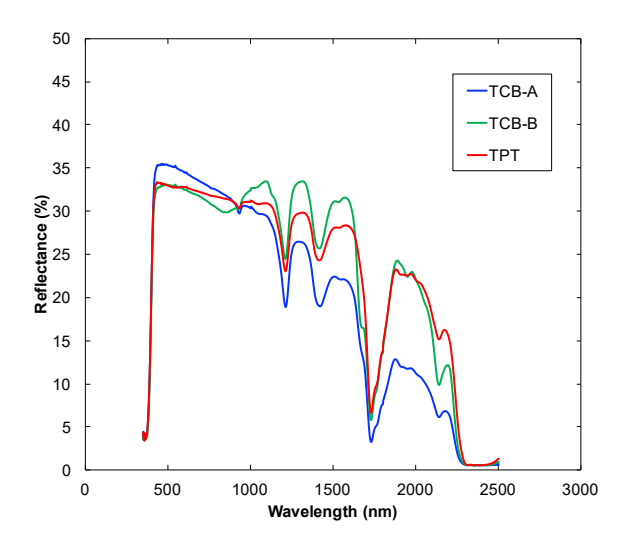


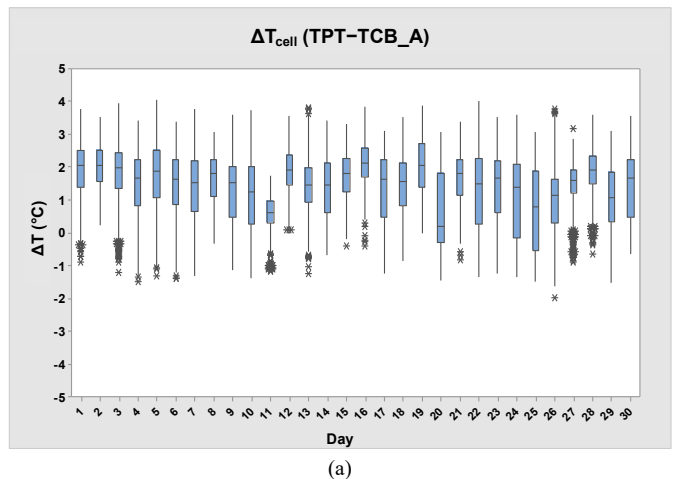
Fig. 6. Reflectance of encapsulated backsheet materials (inner surface) measured on non-cell area backsheet (inner side) through glass of single-cell coupons.

reflectance results indicate that mid- and far-infrared radiations can be better radiated or transmitted by TCB-A than by TPT and TCB-B.

Presently, glass/glass modules are receiving more attention in the PV industry due to multiple reasons: current industrial thinner solar cells tend to break in the field due to a flexible glass/polymer-based module structure; glass/glass modules cause lower material costs than polymeric backsheets; the use of bi-facial solar cells requires a transparent substrate; they provide a higher degree of weatherability. Therefore, glass/glass coupons were also fabricated to compare polymer and glass substrates. As shown in Fig. 4, the determined NOCT of the glass/TPT and glass/glass coupons are approximately 1 °C and 2 °C higher than that of the TCB-A coupons, respectively. It is known that the thermal conductivity of glass is higher than that of the backsheet. However, the thickness of the applied glass is about eight times greater. It was reported that when the substrate thickness is less than 0.5 mm backsheet substrate module would show lower module temperature than the glass substrate module [17]. It may seem that the 1-2 °C decrease in temperature is not significant. However, it is when the lifetime and long-term energy production (i.e., LCOE) of the modules are taken into account since current power plants contain several millions of modules.

C. Module operating temperature

In the previous section, we presented the NOCT values for glass/TPT, glass/TCB-A, glass/TCB-B, and glass/glass coupons. It is to be noted that the NOCT of a module represents the temperature of the cell only at a single set of weather conditions: an irradiance of 800 W/m², an ambient temperature of 20 °C, and an average wind speed of 1 m/s. In order to predict the energy production and lifetime of the PV modules, it is necessary to evaluate the cell temperature difference ($\Delta T_{\rm cell}$) at various sets of weather conditions. Therefore, multiple $\Delta T_{\rm cell}$ values for several consecutive days were investigated. Fig. 7 shows $\Delta T_{\rm cell}$ in a box plot. To generate these plots, the data



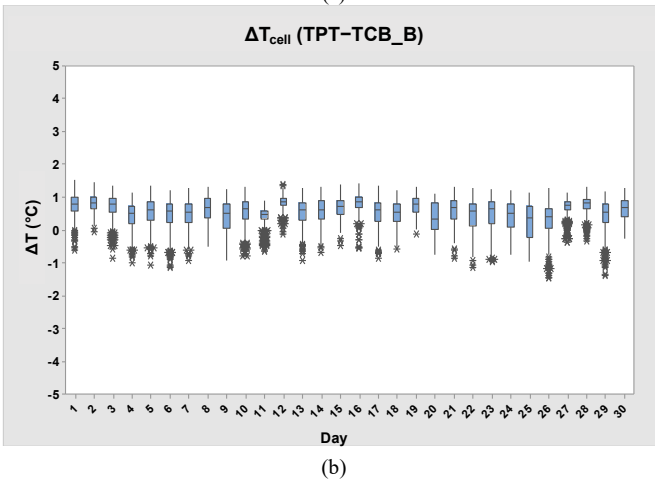


Fig. 7. (a) ΔT_{cell} (TPT-TCB_A) at ASU-PRL, and (b) ΔT_{cell} (TPT-TCB_B) in Mesa, Arizona, June 2017; two TPT temperatures and two TCB temperatures were averaged, respectively.

process was limited to the following weather conditions: >400 W/m² irradiance, >0.25 m/s wind speed, and 9 am–3 pm.

Similar to the NOCT results (section B), overall TCB-A and TCB-B median cell temperatures are approximately 2 °C and 0.8 °C lower than that of TPT, respectively. Moreover, during days with high irradiance levels, the TCB-A ΔT_{cell} is as much as 4 °C cooler than that of the TPT baseline as shown in Fig. 7(a). These are remarkably high values as opposed to the modeled values [8]. As a matter of fact, using TCB in field-operated PV modules shows very promising results in reducing the cell temperature, as shown in Fig. 7, not only on clear sunny days but also on partially cloudy days (June 6th–10th, 20th, and 25th).

Fig. 8(a) and Fig. 8(b) show the daily average ΔT_{cell} and daily average $\Delta T_{backsheet}$ for the TPT/TCB-A and TPT/TCB-B coupons, respectively. As shown in Fig. 8(a), in June 2017, 27 out of 30 days exhibit a daily average ΔT_{cell} (TCB-A) above 1 °C, and an average ΔT_{cell} above 2 °C is observed from three days. As shown in Fig. 8(b), TCB-B is not as effective as TCB-A, but an overall cooling effect compared to the TPT values is measurable. In Fig. 8(a) and Fig. 8(b), it can be observed that the overall average daily ΔT_{cell} is 0.2–0.4 °C higher than $\Delta T_{backsheet}$. This difference is primarily attributed to the convective cooling by the air flow on the air side of the

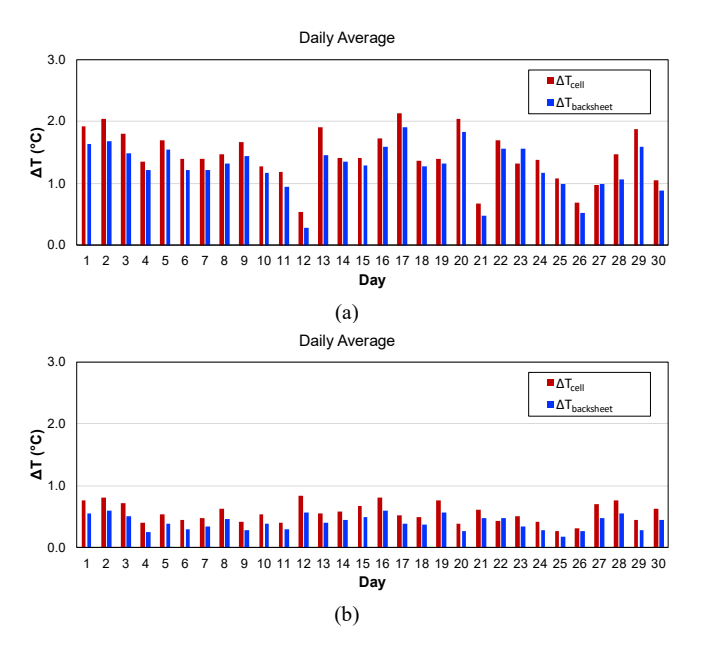
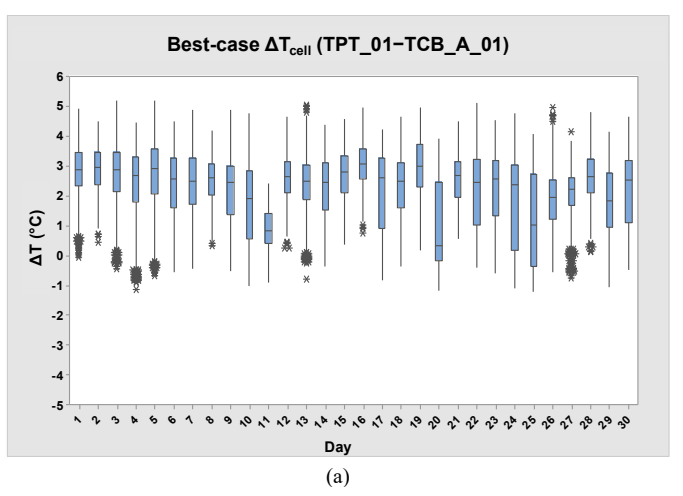


Fig. 8. Daily average ΔT_{cell} and $\Delta T_{backsheet}$ in June 2017, Mesa, Arizona. (a) ΔT of TCB-A, (b) ΔT of TCB-B.

backsheet. The plot clearly indicates that the energy gain, due to the use of TCB, shall be accounted for being based on the ΔT_{cell} as opposed to $\Delta T_{backsheet}$.

In Fig. 7 and Fig. 8, the average ΔT is presented based on the average values of two TCB coupons (two TCB-A coupons or two TCB-B coupons), and the average values of two TPT coupons. Fig. 9 shows the highest ΔT based on the best



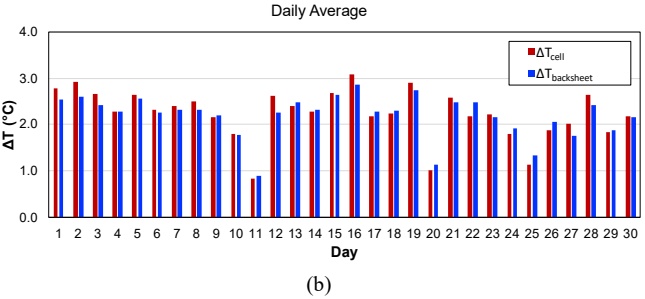


Fig. 9. ΔT based on the best performing TCB (out of four) and worst performing TPT (out of two) in June 2017, Mesa, Arizona. (a) ΔT_{cell} , (b) daily average ΔT_{cell} and $\Delta T_{backsheet}$.

performing TCB (out of four) and worst performing TPT (out of two). Fig. 9 indicates that ΔT can easily exceed 2 °C on clear sunny days during the hot summer months, which accounts for more than 23 days during June in Mesa, Arizona. As shown for the days 11, 20, and 25 in Fig. 9, ΔT can fall below 2 °C (even below 1 °C) during cloudy or overcast days with high wind speed. It is noteworthy that ΔT in Fig. 9(a) can be as high as 5 °C during very sunny periods of very hot days. The exact physical reason for these temperature fluctuations has yet to be investigated with statistical significance and will be the subject of future research.

D. Thermal model

Based on the measured cell temperatures and weather data, an empirical thermal model (see Equation (1)) was developed using a linear-regression approach. Three input parameters—irradiance, ambient temperature, and wind speed—were used in this linear-regression model. Other environmental factors such as wind direction and relative humidity were neglected here since these two factors are considered to have negligible impacts on the cell temperature [22]. The thermal model was developed based on data collected between 7 am–6 pm during two periods: May 1–31, 2017 (six glass/backsheet modules), and June 9–July 12, 2017 (six glass/backsheet modules and two glass/glass modules). Owing to unexplainable technical issues, the data collected during certain days—May 8, June 12, July 5, and July 11—were not considered for the model development.

$$T_{cell} = w_1 \cdot E + w_2 \cdot T_{amb} + w_3 \cdot WS + c \tag{1}$$

Where.

 T_{cell} : cell temperature (°C) E: irradiance (W/m²)

 T_{amb} : ambient temperature (°C)

WS: wind speed (m/s) w_1, w_2, w_3 : coefficients

c: constant.

The coefficients obtained for the parameters in (1) are provided in Table III and it can be noted that the cell temperature is primarily dictated by the ambient temperature regardless of the substrate type, as shown in Table III. The base temperature of the cell is set by the ambient temperature, and the irradiance (solar gain) is responsible for the cell temperature rise of 0.030 °C per W/m², 0.031 °C per W/m², and 0.032 °C per W/m² (average irradiance coefficients) for TCB-A, TCB-B, and TPT, respectively. Based on this thermal model and the w₁coefficients presented in Table III, it can be determined that T_{cell} of TCB-A would be 2 °C lower than that of TPT at a 1000 W/m² irradiance level. In other words, the cell temperature of TCB-A is less affected by the irradiance increase than that of TPT. The T_{amb} coefficient (w₂) and wind speed coefficient (w₃) keep basically constant irrespective of the backsheet type (TPT, TCB-A, or TCB-B). Thus, it can be concluded that the irradiance (solar gain) is a primary factor that differentiates between backsheet types. The solar gain can be decreased by increasing the conductive and radiative cooling of the backsheet

TABLE III
THERMAL MODEL COEFFICIENTS FOR CELL TEMPERATURE DETERMINED
USING FOUNTION 1

Type of Substrate	Coupon	E (w ₁)	T _{amb} (w ₂)	WS (w ₃)	С
	1	0.0292	0.992	-1.497	1.422
TCB-A	2	0.0308	1.002	-1.471	0.791
	Average	0.0300	0.997	-1.484	1.106
	1	0.0314	0.995	-1.463	0.511
TCB-B	2	0.0311	1.019	-1.415	0.300
	Average	0.0312	1.007	-1.439	0.406
	1	0.0317	1.010	-1.472	0.703
TPT	2	0.0314	0.998	-1.376	0.747
	Average	0.0315	1.004	-1.424	0.725
Backsheet average		0.0309	1.003	-1.449	0.746
	1	0.0317	0.989	-1.202	1.402
Glass	2	0.0331	1.059	-1.089	-1.933
	Average	0.0324	1.024	-1.146	-0.265

materials as demonstrated in this work. For glass/glass and glass/TPT coupons, the average w₁ and w₂ are practically identical. However, the average w₃ of glass/glass modules is by more than 30 % lower than that of any polymer backsheet module. This indicates that wind speed causes a higher reduction in the cell temperature in polymer substrate modules than in glass substrate modules. Compared to TPT-based modules, glass/glass-based modules are expected to show 0.6 °C higher cell temperatures at wind speeds of 2 m/s, which is frequently encountered in the field. In summary, the primary differentiator for temperature differences regarding TPT, TCB,

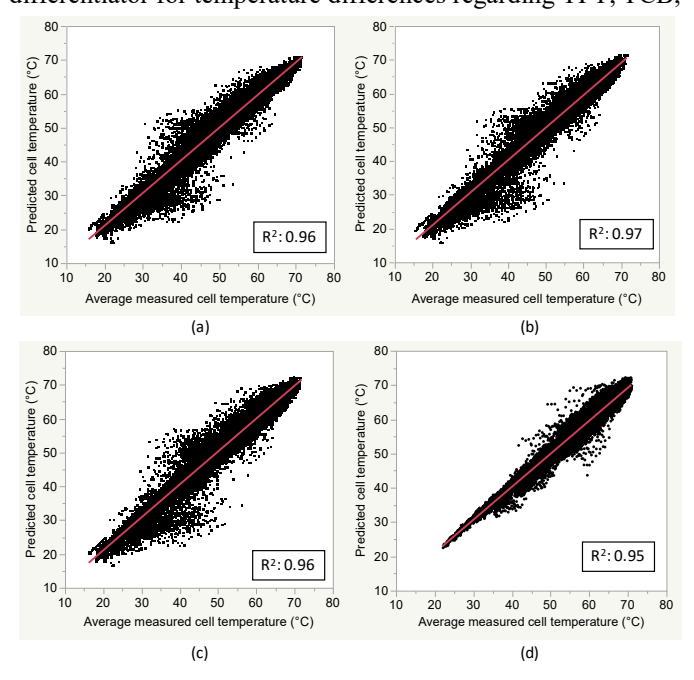


Fig. 10. Predicted cell temperature as function of averaged measured cell temperature using proposed thermal model. (a) TCB-A, (b) TCB-B, (c) TPT, (d) glass/glass.

and glass substrates appears to be the irradiance level (solar gain due to reduced radiative and conductive losses). In addition, the wind speed level plays secondary role for the temperature difference regarding backsheets and glass substrates, but not between backsheet types.

To visualize the validity of the proposed thermal model for a wide range of conditions and days, the predicted cell temperature was plotted against the actual temperature, as shown in Fig. 10. The trend lines of all plots in Fig. 10 have a good fit, as indicated by the high R² values. It should be noted that more scattered points of the predicted cell temperature at average measured cell temperature between 30 °C–50 °C (see Fig. 10 (a)–(c)) are due to moving clouds causing a sudden irradiance drop. These plots clearly indicate that the thermal model developed and presented in this work should be sufficient to predict cell temperatures based on the measured weather parameters.

Simple 2D physical thermal model was also developed using ANSYS. As shown in Table IV, ΔT_{cell} of TCB-A is 0.623 °C at NOCT condition (800 W/m² POA irradiance, 20 °C ambient temperature, 1 m/s wind speed). This is about 50% lower than ΔT_{cell} shown in Fig. 4, however it still shows lower temperature than TPT as observed in the experimental results. TCB-B did not show reduced temperature compared to TPT at <2 m/s wind speed in the model while the actual NOCT of TCB-B was 0.7 $^{\circ}$ C lower than TPT. The modeled ΔT_{cell} at NOCT were also compared with real time measured ΔT_{cell} with ambient condition identical to NOCT condition. As shown in Fig. 11, instant measured ΔT_{cell} is ranged up to ± 2 °C that is common in NOCT analysis, and the modelled ΔT_{cell} is within the range and is close to the measured median. In the empirical thermal model we indicated that the effect of wind speed among backsheets (TPT and TCBs) is not the dominant factor in increasing ΔT_{cell} for this narrow wind speed range site, which may not be the case in high wind speed range site. However, this thermal model result shows that ΔT_{cell} is influenced by the wind speed. To explain this difference, a complex 3D thermal model representing multi-cell commercial PV module using ANSYS is in progress to fully understand the effect of TCB on cell temperature and that is the subject of a future publication.

IV. SUMMARY AND CONCLUSIONS

In this study, thermal conductivity and emissivity were experimentally determined for a TPT and two TCB materials. Both investigated TCB products are determined to have approximately twice the axial thermal conductivity compared to the TPT baseline. TCB-B exhibited an extremely high radial thermal conductivity—most likely due to the presence of a thin inner aluminum layer within its material stack, but it showed lower emissivity than TPT. Multiple single-cell coupons were fabricated with TCB, TPT, and glass substrates to evaluate their thermal performance. The single-cell coupons were installed on an open rack following the NOCT test conditions: 45° fixed tilt and south-facing. It was observed that the NOCT of the TCB-A coupon was 1.2 °C lower than that of the TPT coupon. However, the NOCT of the glass/glass coupon was rather 0.9 °C higher than that of the TPT coupon due to the thickness of

TABLE IV SIMULATED ΔT_{CELL} AT NOCT CONDITION (800 W/m² POA IRRADIANCE, 20 °C AMBIENT TEMPERATURE)

Wind speed (m/s)	ΔT _{cell} TPT-TCB_A (°C)	ΔT _{cell} TPT-TCB_B (°C)
0	0.954	-0.100
1	0.623	-0.020
2	0.446	0.022

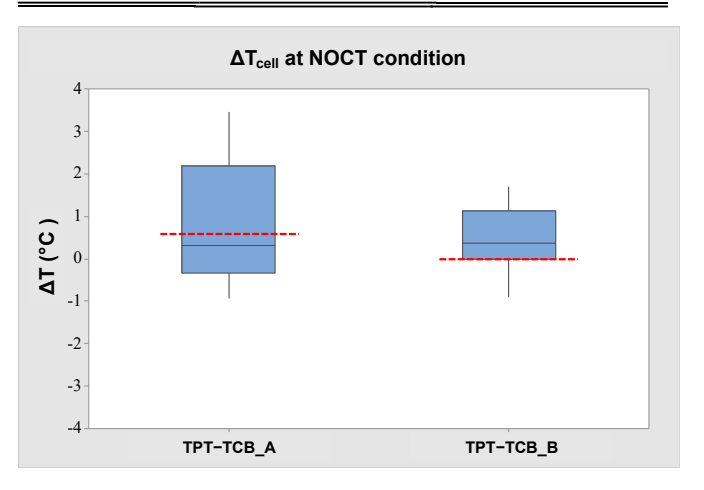


Fig. 11. Model validation: Thirty-nine instantly measured ΔT_{cell} over one year at NOCT condition for TCB-A and TCB-B single-cell coupons are shown in the boxplot. Dotted red lines indicate ΔT_{cell} (at NOCT condition) modelled by ANSYS.

the glass although glass substrate has a higher thermal conductivity than TCB backsheet. These finding are expected to be highly beneficial to the industry that is currently preparing itself to build more and more glass/glass PV modules. Module operating temperature for glass/backsheet modules were collected during summer in Mesa, Arizona. We demonstrated that backsheet materials with an increased thermal conductivity contribute to a decrease in the average cell temperature of more than 1 °C in general, and of more than 2 °C on hot sunny days. Furthermore, the TCB coupon lowers the cell temperature as much as 5 °C compared to a TPT coupon during a few hot and sunny summer days. This work confirms that both thermal conductivity and emissivity of the backsheet play an important role in lowering cell temperature of the PV modules. Based on the collected data, an empirical thermal model was developed using linear regressions that compares the effects of irradiance, ambient temperature, and wind speed on the cell temperature. A simple physical thermal model was developed using ANSYS and it shows that TCB-A cell temperature at NOCT condition is about 0.6 °C lower than TPT cell temperature. However, since the current model only includes a 2D cross-section of single-cell coupons neglecting its actual design having significant non-cell area (see Fig. 2), the modelled TCB-B cell temperature is observed to be slightly higher than TPT. Therefore, this model needs to be further improved to account for the role of higher radial thermal conductivity existing in TCB-B. Modelled values are still within the acceptable range of the field measured data.

ACKNOWLEDGEMENT

The authors would like to thank T. Silverman of National Renewable Energy Laboratory for emissivity measurement and A. Parikh of WindLogics for assistance with physical thermal model.

REFERENCES

- [1] M. A. Green, Solar cells: operating principles, technology, and system applications. New Jersey: Prentice-Hall, 1982.
- [2] H. A. Hussien, A. H. Numan, and A. R. Abdulmunem, "Improving of the photovoltaic / thermal system performance using water cooling technique," in *IOP Conference Series: Materials Science and Engineering*, 2015, vol. 78, no. 1.
- [3] C. G. Popovici, S. V. Hudişteanu, T. D. Mateescu, and N.-C. Cherecheş, "Efficiency Improvement of Photovoltaic Panels by Using Air Cooled Heat Sinks," *Energy Procedia*, vol. 85, pp. 425–432, 2016.
- [4] H. G. Teo, P. S. Lee, and M. N. A. Hawlader, "An active cooling system for photovoltaic modules," *Appl. Energy*, vol. 90, no. 1, pp. 309–315, 2012.
- [5] B. Lee, J. Z. Liu, B. Sun, C. Y. Shen, and G. C. Dai, "Thermally conductive and electrically insulating EVA composite encapsulant for solar photovoltaic (PV) cell," eXPRESS Polym. Lett., vol. 2, no. 5, pp. 357–363, 2008.
- [6] N. Kim, D. Kim, H. Kang, and Y.-G. Park, "Improved heat dissipation in a crystalline silicon PV module for better performance by using a highly thermal conducting backsheet," *Energy*, vol. 113, pp. 515–520, 2016.
- [7] X. Sun, T. J. Silverman, Z. Zhou, M. R. Khan, P. Bermel, and M. A. Alam, "Optics-Based Approach to Thermal Management of Photovoltaics: Selective-Spectral and Radiative Cooling," *IEEE J. Photovoltaics*, vol. 7, no. 2, pp. 566–574, 2017.
- [8] T. J. Silverman, M. G. Deceglie, I. Subedi, N. J. Podraza, I. M. Slauch, V. E. Ferry, and I. Repins, "Reducing Operating Temperature in Photovoltaic Modules," *IEEE J. Photovoltaics*, vol. 8, no. 2, pp. 532–540, 2018.
- [9] L. Zhu, A. Raman, K. X. Wang, M. A. Anoma, and S. Fan, "Radiative cooling of solar cells," *Optica*, vol. 1, no. 1, pp. 32–38, 2014
- [10] L. Zhu, A. P. Raman, and S. Fan, "Radiative cooling of solar absorbers using a visibly transparent photonic crystal thermal blackbody," *Proc. Natl. Acad. Sci. U. S. A.*, vol. 112, no. 40, pp. 12282–12287, 2015.
- [11] G. Tamizhmani and J. Kuitche, "Accelerated Lifetime Testing of PV Modules," Solar America Board for Codes and Standards, 2013.
- [12] F. Mahmood, H. Majeed, H. Agha, S. Ali, S. Tatapudi, T. Curtis, and G. TamizhMani, "Temperature coefficient of power (Pmax) of field aged PV modules: impact on performance ratio and degradation rate determinations," in SPIE 10370, Reliability of Photovoltaic Cells, Modules, Components, and Systems X, 2017, vol. 10370, pp. 1037007–1037008.
- [13] S. Armstrong and W. G. Hurley, "A thermal model for photovoltaic panels under varying atmospheric conditions," *Appl. Therm. Eng.*, vol. 30, no. 11, pp. 1488–1495, 2010.
- [14] J. Allan, H. Pinder, and Z. Dehouche, "Enhancing the thermal conductivity of ethylene-vinyl acetate (EVA) in a photovoltaic thermal collector," *AIP Adv.*, vol. 6, no. 3, p. 35011, 2016.
- [15] IEC, "Crystalline silicon terrestrial photovoltaic (PV) modules design qualification and type approval." IEC 61215 Ed. 2, 2005.
- [16] J. Zhou, Q. Yi, Y. Wang, and Z. Ye, "Temperature distribution of photovoltaic module based on finite element simulation," *Sol. Energy*, vol. 111, pp. 97–103, Jan. 2015.
- [17] J. Zhou, Z. Zhang, H. Liu, and Q. Yi, "Temperature distribution and back sheet role of polycrystalline silicon photovoltaic modules," *Appl. Therm. Eng.*, vol. 111, no. Supplement C, pp. 1296–1303, 2017.
- [18] H. A. Zondag, D. W. de Vries, W. G. J. van Helden, R. J. C. van Zolingen, and A. A. van Steenhoven, "The yield of different combined PV-thermal collector designs," *Sol. Energy*, vol. 74, no. 3, pp. 253–269, 2003.
- [19] Thermtest Inc., "Materials Thermal Properties Database." [Online]. Available: https://thermtest.com/materials-database.

- [20] A. Pavgi, J. Oh, J. Kuitche, S. Tatapudi, and G. TamizhMani, "Thermal Uniformity Mapping of PV Modules and Plants," in *Photovoltaic Specialists Conference (PVSC)*, 2017 44th IEEE, 2017.
 [21] J. Oh, A. Pavgi and G. TamizhMani, "Determination of Empirical
- [21] J. Oh, A. Pavgi, and G. TamizhMani, "Determination of Empirical Coefficients and ΔT for Sandia Thermal Model: Dependence on Backsheet Type," in 7th World Conference on Photovoltaic Energy Conversion (WCPEC-7), abstract accepted, 2018.
- [22] Y. Tang, "Outdoor Energy Rating Measurements of Photovoltaic Modules," Master's thesis, Arizona State University, 2005.